
Balance of Number of Embedding and their Dimensions in Vector Quantization

Hang Chen

BeiJing JiaoTong University
22120028@bjtu.edu.cn

Sankepally Sainath Reddy

Indian Institute of Technology
sankepallysainathreddy@gmail.com

Ziwei Chen

BeiJing JiaoTong University
zwchen@bjtu.edu.cn

Dianbo Liu

National University of Singapore
dianbo@nus.edu.sg

Abstract

The dimensionality of the embedding and the number of available embeddings (also called codebook size) are critical factors influencing the performance of Vector Quantization (VQ), a discretization process used in many models such as the Vector Quantized Variational Autoencoder (VQ-VAE) architecture. This study examines the balance between the codebook sizes and dimensions of embeddings in VQ, while maintaining their product constant. Traditionally, these hyper parameters are static during training; however, our findings indicate that augmenting the codebook size while simultaneously reducing the embedding dimension can significantly boost the effectiveness of the VQ-VAE. As a result, the strategic selection of codebook size and embedding dimensions, while preserving the capacity of the discrete codebook space, is critically important. To address this, we propose a novel adaptive dynamic quantization approach, underpinned by the Gumbel-Softmax mechanism, which allows the model to autonomously determine the optimal codebook configuration for each data instance. This dynamic discretizer gives the VQ-VAE remarkable flexibility. Thorough empirical evaluations across multiple benchmark datasets validate the notable performance enhancements achieved by our approach, highlighting the significant potential of adaptive dynamic quantization to improve model performance.

1 Introduction

The Vector Quantized-Variational Autoencoder (VQ-VAE) (Van Den Oord et al., 2017), which blends the methodologies of Variational Autoencoders (VAEs) (Kingma and Welling, 2013) and Vector Quantization (VQ) (Gray, 1984), effectively tackles the issue of noisy reconstructions commonly associated with VAEs by learning data representations that are both compact and efficient. In the VQ-VAE architecture, a vector quantization (VQ) layer converts continuous embeddings z_e into their discrete equivalents z_q . Due to the non-differentiable nature of the discretization process, the straight-through estimator (STE) (Bengio et al., 2013) is used to perform backpropagation. The codebook, which stores these discrete values, has been a focal point of significant research aimed at addressing codebook collapse, a challenge introduced by the use of STE. Innovative techniques such as the use of Exponential Moving Average (EMA) (Van Den Oord et al., 2017) and the introduction of multi-scale hierarchical structures in the VQ-VAE-2 (Razavi et al., 2019) have proven effective in improving codebook efficiency.

A variety of techniques have been utilized to enhance the diversity of codebook selections and alleviate issues of underutilization. These methods include stochastic sampling (Roy et al., 2018;

Kaiser et al., 2018; Takida et al., 2022), repeated K-means (MacQueen et al., 1967; Łańcucki et al., 2020), and various replacement policies (Zeghidour et al., 2021; Dhariwal et al., 2020). Furthermore, studies have investigated the impact of codebook size on performance. For example, Finite Scalar Quantization (FSQ) (Mentzer et al., 2023) achieves comparable performance to VQ-VAE with a reduced quantization space, thereby preventing codebook collapse. Similarly, Language-Free Quantization (LFQ) (Yu et al., 2023) minimizes the embedding dimension of the VQ-VAE codebook to zero, improving reconstruction capabilities. The VQ optimization technique (Li et al., 2023) allows for adjustments in codebook size without necessitating retraining, addressing both computational limits and demands for reconstruction quality. Despite these significant developments, an automated approach to determine the ideal codebook size and dimension of each codeword for specific datasets and model parameters remains unexplored.

This research tackles the fore-mentioned gap by exploring the ideal codebook size for VQ-VAE. We present three major contributions:

- **Optimal Codebook Size and Embedding Dimension Determination:** We systematically explored different combinations of codebook size and embedding dimension to understand optimal balances for different tasks.
- **Adaptive Dynamic Quantization:** We introduce novel quantization mechanism that enables data points to autonomously select the optimal codebook size and embedding dimension.
- **Empirical Validation and Performance Enhancement:** We conducted thorough empirical evaluations across multiple benchmark datasets to understand behaviors of the dynamic quantizer.

2 Preliminaries

In this study, x is the input data, \hat{x} is the output data, $E(\cdot)$ is the encoding function, $G(\cdot)$ is the decoding function, and $\mathcal{L}(\cdot)$ is the loss function.

2.1 Vector-quantized networks

A VQ-VAE network comprises three main components: encoder, decoder and a quantization layer $h(\cdot)$.

$$\hat{x} = G(h(E(x))) = G(h(z_e)) = G(z_q) \quad (1)$$

The VQ layer $h(\cdot)$ quantizes the vector $z_e = E(x)$, by selecting one vector from N vectors so that $z_q = h(z_e)$. These N candidate vectors are called code embeddings or codewords, and they are combined to form a codebook $C = \{c_1, c_2, c_3 \dots c_N\}$.

In codebook C , each code vector has a fixed index. Therefore, for the quantization layer, the discrete embedding z_q that z_e is quantized into is selected from the N code vectors in the codebook, $z_q \in R^{T \times D}$, D is the embedding dimension and T refers to the number of data points. This selection process is implemented using the nearest neighbor method:

$$z_q = c_k, \quad \text{where } k = \underset{j}{\operatorname{argmin}} \|z_e - c_j\|_2 \quad (2)$$

In this process, P_Z is represented as the data distribution after being encoded by the encoder, and Q_Z represents the data distribution in the codebook space. After quantization, z_q is used to predict the output $\hat{x} = G(z_q)$, and the loss is computed with the target $x : L(\hat{x}, x)$. The above introduces the data flow process of a single vector passing through the VQ-VAE model. For images, VQ is performed at each spatial location on the existing tensor, where the channel dimensions are used to represent vectors. For example, the graphical data of $z_e \in R^{B \times C \times H \times W}$ is flattened into $z_e \in R^{(B \times H \times W) \times C}$, and then it goes through the process $z_e \in R^{(B \times H \times W) \times C} \xrightarrow[\text{projection}]{h(\cdot)} z_q \in R^{T \times D}$, $T = B \times H \times W$. B , C , H and W are the batch size, number of channels, image height,

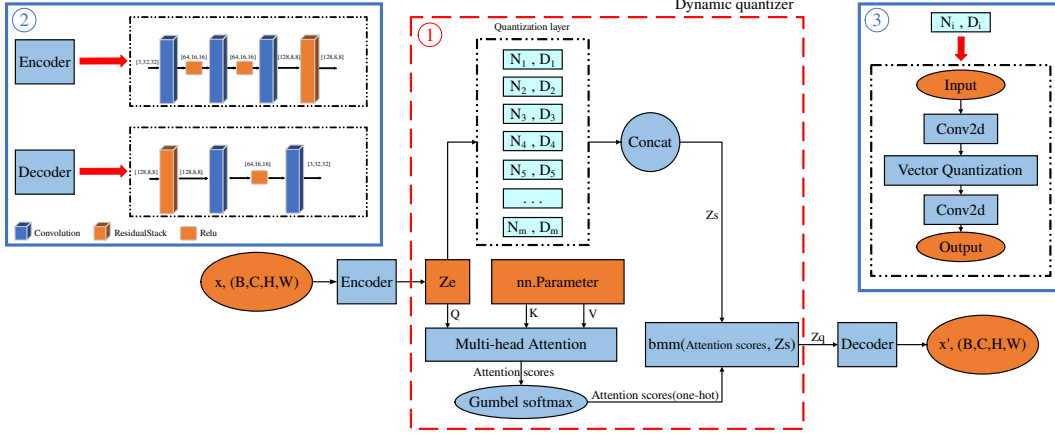


Figure 1: Schematic diagram of VQ-VAE network with adaptive dynamic quantization structure: (1)Utilizes the multi-head "attention mechanism" and Gumbel-Softmax operation to achieve dynamic selection of the quantization codebook. (2)Both the encoder and decoder employ CNN+ResNet architectures. (3)The experimental model includes functions for dimension transformation before and after quantization within the quantization layer to facilitate data flow.

and width of image data, respectively. The standard training objective of VQ-VAE is to minimize reconstruction loss, its total loss is:

$$\mathcal{L} = \mathcal{L}_{task} + \mathcal{L}_{cmt} = \|x - \hat{x}\|_2^2 + \beta \{ \|sg[z_e] - z_q\|_2^2 + \alpha \|z_e - sg[z_q]\|_2^2 \} \quad (3)$$

Including the terms with $sg[\cdot]$ which is stop-gradient operation, in the two items are the commitment loss. The gradient through non-differentiable step is calculated using straight-through estimation $\frac{\partial \mathcal{L}}{\partial E} = \frac{\partial \mathcal{L}}{\partial z_q} \frac{\partial z_q}{\partial E} \approx \frac{\partial \mathcal{L}}{\partial z_q} \frac{\partial z_q}{\partial z_e} \frac{\partial z_e}{\partial E}$ is accurate. α is a hyperparameter and set to 0.25. β is a parameter that controls the proportion of quantization loss. Exponential Moving Average (EMA) is a popular approach to update the codebook according to values of the encoder outputs: $\mathbf{z}_q^{(t+1)} \leftarrow (1 - \gamma) \cdot \mathbf{z}_q^{(t)} + \gamma \cdot \mathbf{z}_e^{(t)}$, where γ is the decay coefficient.

2.2 Related work

Vector Quantization (VQ) is a prominent technique in deep learning for deriving informative discrete latent representations. As an alternative to VQ, Soft Convex Quantization(Gautam et al., 2023) solves for the optimal convex combination of codebook vectors during the forward pass process. Various methods, such as HQ-VAE(Takida et al., 2023), CVQ-VAE(Zheng and Vedaldi, 2023), HyperVQ(Goswami et al., 2024), and EdVAE(Baykal et al., 2023), have been developed to enhance the efficiency of codeword usage, achieve effective latent representations, and improve model performance. The Product Quantizer(Baldassarre et al., 2023) addresses the issue of local significance by generating a set of discrete codes for each image block instead of a single index. One-Hot Max (OHM)(Löhdefink et al., 2022) reorganizes the feature space, creating a one-hot vector quantization through activation comparisons. The Residual-Quantized VAE(Lee et al., 2022) can represent a 256×256 image as an 8×8 resolution feature map with a fixed codebook size. DVNC(Liu et al., 2021) improves the utilization rate of codebooks through multi head discretization. The following DVQ(Liu et al., 2022) dynamically selects discrete compactness based on input data. QINCo(Huijben et al., 2024), a neural network variant of residual quantization, uses a neural network to predict a specialized codebook for each vector based on the vector approximation from the previous step. Similarly, this research utilizes an attention mechanism(Vaswani et al., 2017) combined with Gumbel-Softmax to ensure the selection of the most suitable codebook for each data point.

3 Method

3.1 Codebook structure search

To investigate the impact of codebook size and embedding dimension on VQ-VAE’s performance while maintaining a fixed capacity of the discrete information space, we conducted a series of experiments with various combinations of codebook sizes and embedding dimensions.. We denote the number of codewords by N and the embedding dimension by D . For a given discrete information space capacity W , the possible codebook structures are represented as $H = \{[N_1, D_1], [N_2, D_2], \dots, [N_m, D_m]\}$, where $N_i \times D_i = W$ and $N_i, D_i \in \mathbb{N}^+$. **In this study, we fix W and explore different combination of N and D .**

For these codebook combinations, we ensure that the number of codewords N is always greater than the embedding dimension D for two reasons: (1) a small number of codewords can significantly degrade the model’s performance. (2) maintaining consistency in subsequent experiments. These systematic experiments aim to validate our hypothesis that the codebook size influences model performance and its pattern of impact. We hypothesize that increasing the number of codewords can enhance the reconstruction performance of VQ-VAE. Based on the results obtained from exploring different codebook combinations, further refined experiments are detailed in Section 3.2.

3.2 Adaptive dynamic quantization mechanism

Unlike methods that use a single fixed codebook, our approach utilizes multiple codebooks while ensuring that the product of the codebook size and the embedding dimension remains constant. The diagram of our experimental model is presented in Figure 1. The detailed algorithm of VQ-VAE with Adaptive Dynamic Quantization is clearly depicted in Algorithm 1. A pool of m discretization

Algorithm 1 VQ-VAE with Adaptive Dynamic Quantization.

- 1: **Input:** Original images x , Number of embeddings $num_embeddings$, Embedding dimension $embedding_dims$, Hidden layer dimension $num_hiddens$
 - 2: **Output:** Reconstructed images \hat{x} , Reconstruction loss L
 - 3: Randomly initialize K with sizes $[m, 1, num_hiddens]$.
 - 4: Encoder $E(\cdot)$, Decoder $G(\cdot)$, Quantization layers $h_i(\cdot), i \in \{1, 2, 3, \dots, m\}$, Gumbel-Softmax function $GS(\cdot)$
 - 5: $z_e = E(x)$
 - 6: $Q = z_e.flatten(-1, num_hiddens)$
 - 7: One-hot selection score: $scores = GS(MultiHead(Q, K))$
 - 8: $z_q^i, vq_loss_i = h_i(z_e)$
 - 9: $z_s = concat[z_q^1, z_q^2, \dots, z_q^m]$, $extraloss = \frac{1}{m} \sum_{i=1}^m vq_loss_i$
 - 10: $z_q = BMM(scores, z_s)$
 - 11: $\hat{x} = G(z_q)$
 - 12: $recon_loss = MSE(x, \hat{x}), L = recon_loss + extraloss$.
-

codebooks $H = \{[N_i, D_i]\}_{i \in [m]}$ is provided for all representations undergoing discretization. Each codebook $[N_i, D_i]$ is associated with a unique quantization layer $h_i(\cdot)$. These discretization codebooks and their corresponding quantization layers are independent and do not share parameters. The discrete vector obtained by quantizing z_e through the quantization layer $h_i(\cdot)$ is denoted as z_q^i . Each quantizer $h_i(\cdot)$ possesses a unique key vector k_i and value vector v_i , which are initially randomly initialized. To perform parameter feature learning for the quantization layers, we utilize the Multi-Head Attention mechanism, defined as $scores_{attention} = MultiHead(Q, K, V)$, where Q is the flattened vector of z_e and $K = concat(k_1, k_2, \dots, k_m)$, $V = concat(v_1, v_2, \dots, v_m)$. The Gumbel-Softmax operation is applied to the attention scores for one-hot selection to determine which codebook to use, with the categorical distribution given by $\pi^{z_e}(i) = \frac{\exp(k_i^\top z_e)}{\sum_{j \in [N]} \exp(k_j^\top z_e)}$.

Finally, the attention scores obtained after the Gumbel-Softmax operation are combined with multiple quantized vectors to produce the final quantized vector z_q . This is achieved using batch matrix multiplication, denoted as $z_q = BMM(scores_{attention}, z_s)$, where $z_s = concat(z_q^1, z_q^2, \dots, z_q^m)$. The

Table 1: Reconstruction loss under different fixed codebook models

[N,D]	Datasets					
	MNIST	FshionMNIST	CIFAR10	Tiny-ImageNet	Diabetic-retinopathy	CelebA
[512,128]	0.285	0.577	0.606	2.679	0.361	0.177
[1024,64]	0.294	0.590	0.663	2.654	0.400	0.156
[2048,32]	0.291	0.602	0.618	2.640	0.410	0.155
[4096,16]	0.265	0.589	0.618	2.650	0.362	0.136
[8192,8]	0.240	0.503	0.553	2.605	0.337	0.122
[16384,4]	0.210	0.489	0.503	2.528	0.347	0.120
[32768,2]	0.199	0.578	0.808	3.364	0.407	0.171
[65536,1]	0.377	0.877	1.353	4.631	0.493	0.334

loss function for this dynamic quantization-based VQ-VAE model is given in Equation 4.

$$\mathcal{L} = \|x - \hat{x}\|_2^2 + \frac{1}{m} \sum_{i=1}^m \beta \{ \|sg[z_e] - z_q^i\|_2^2 + \alpha \|z_e - sg[z_q^i]\|_2^2 \} \quad (4)$$

4 Experimental results and analysis

All our experiments were conducted with a constant information capacity for the codebooks. This means that while the sizes of the codebooks and the embedding dimensions varied, their product remained constant, ensuring the discrete space capacity stayed unchanged. We experimented with six datasets: MNIST, FashionMNIST, CIFAR-10, Tiny-Imagenet, CelebA, and a real-world dataset, the Diabetic Retinopathy dataset. In the experiments described in Sections 4.1 and 4.2, the discrete information space size of the experimental model was set to 65536. The multi-head attention mechanism used had two heads. The codebook in the VQ operation was updated using the EMA method. Both the encoder and decoder architectures were designed with Convolutional Neural Networks(CNN)(LeCun et al., 1998) and Residual Network(ResNet)(He et al., 2016). The hyperparameters α , β , and γ were set to 0.25, 1, and 0.99, respectively. Part of the experimental results are presented in Section 4, please refer to the Appendix for other results.

4.1 The influence of codebook size and embedding dimension

Before enhancing the quantization method of the VQ-VAE, we conducted an in-depth analysis on how various combinations of codebook size N and embedding dimensions D affect the model’s performance. This study was carried out with the constraint that the capacity of the discrete space in the VQ-VAE model remained constant, meaning that the product of N and D was kept unchanged. In the original VQ-VAE model configuration, we specified a codebook size of 512 and embedding dimensions of 128. From this starting point, we transitioned to experimenting with various other combinations of N (codebook size) and D (embedding dimensions), ranging from [1024, 64] to [65536, 1], to observe their individual effects on the model’s performance. Our findings indicate that increasing N , the codebook size, generally enhances the model’s performance. However, maintaining a sufficiently high D , the embedding dimension, is also essential to sustain this improvement. The results from these investigations are displayed in Table 1, which outlines the reconstruction loss on the validation set for various N, D configurations, each maintained under identical training conditions across six datasets. Table 1 illustrates that smaller embedding dimensions in the codebook do not always lead to better results. In the original VQ-VAE model, while the codebook size remains constant, modifying it and retraining can yield varied outcomes. Furthermore, within a fixed discrete information space, there is an optimal codebook size that best fits the specific dataset. Following these findings, we computed the terminal gradient gap(Huh et al., 2023) for models that use a consistent codebook size throughout their training. A successful quantization function $h(\cdot)$ retains essential information from a finite vector set z_e . The quantized vector is expressed as $z_q = z_e + \varepsilon$, where ε is the residual vector derived from the quantization process. If $\varepsilon = 0$, it implies no direct estimation error, suggesting that the model effectively lacks a quantization function. Equation 5

describes how to measure the gradient gap concerning this ideal, lossless quantization function.

$$\Delta Gap = \left\| \frac{\partial \mathcal{L}_{\text{task}}(G(\mathbf{z}_e))}{\partial E(x)} - \frac{\partial \mathcal{L}_{\text{task}}(G(\mathbf{z}_q))}{\partial E(x)} \right\| \quad (5)$$

During the training phase, we monitored the variations in the gradient gap. Notably, the pattern of gradient gap changes associated with the codebook remained consistent across three-channel datasets. For instance, we demonstrated the evolving pattern of the gradient gap for the CIFAR10 dataset in Figure 2(left). Although the gradient gap changes are quite similar between two single-channel datasets, differences emerge when comparing single-channel and three-channel datasets. More comprehensive details on these differences are discussed in the Appendix. The reconstruction

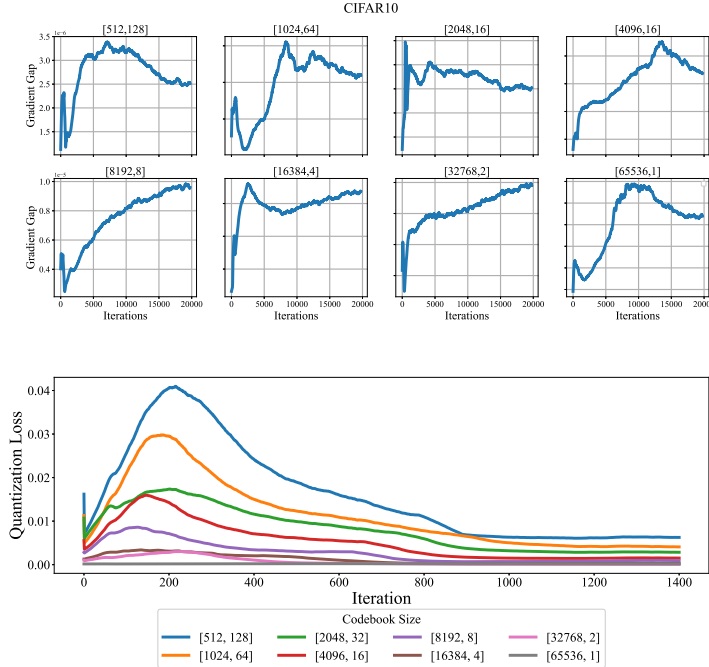


Figure 2: Gradient gap and quantization loss under fixed codebook models.

loss for the other three datasets shows a similar trend. As the codebook size increases up to the point of achieving the lowest validation loss, the gradient gap remains constant. However, once the size surpasses this optimal codebook combination, any further decrease in embedding dimension results in a progressive increase in the gradient gap for subsequent models. From the findings in Table 1, we conclude that within a fixed discrete information space, enlarging the codebook size to a certain extent can enhance the model’s reconstruction capabilities. Nonetheless, if the embedding dimension becomes too small, it will lead to an increased quantization gradient gap, which could degrade the model’s performance rather than enhance it.

Given that each batch contains an equal number of data points, the quantization loss is impacted by the embedding dimension. A smaller embedding dimension tends to yield a reduced quantization loss, as depicted in Figure 2(right).

Analysis: Increasing N generally allows the model to capture more variability in the data due to a larger number of vectors available for encoding the data, potentially reducing quantization error. However, as N increases, the dimension D typically decreases to manage computational complexity and memory usage, which can affect the quality of each individual representation. Lower D might lead to loss of information, since each vector has less capacity to encapsulate details of the data. However, too high a dimension could also mean that the vectors are too specific, reducing their generalizability. As N increases, each vector in the codebook needs to handle less variance, theoretically reducing the reconstruction loss. However, each vector also has fewer D to capture that variance as N decreases. The balance between these factors is delicate and dataset-specific. The characteristics of each dataset heavily influence the optimal N and D . Simpler datasets with

Table 2: Comparison of reconstruction performance between adaptive dynamic quantization model and optimal fixed codebook model.

Models	Datasets					
	MNIST	FshionMNIST	CIFAR10	Tiny-ImageNet	Diabetic-retinopathy	CelebA
Fixed Codebook	0.199	0.489	0.503	2.528	0.337	0.120
Adaptive Codebook	0.166	0.410	0.394	2.022	0.294	0.099

less intrinsic variability (like MNIST) can be effectively modeled even with lower D , while more complex datasets require either higher D or more carefully balanced D .

4.2 Adaptive dynamic quantization mechanism

The adaptive dynamic quantization mechanism allows each data point in a batch to independently select the most appropriate codebook for quantization and training. Mirroring the format seen in Table 1, we have showcased in Table 2 the comparison of reconstruction loss between the best fixed codebook model and an adaptive dynamic quantization model across various validation datasets. Even with an optimized fixed quantization codebook for reconstruction performance, it falls short compared to our proposed adaptive dynamic quantization model. This is because our model allows each input data point to choose from eight codebooks within a discrete information space of 65536 possibilities, whereas the fixed codebook model offers no such flexibility.

The main advantage of our method lies in its ability to learn the distribution of different features in the dataset and adapt to the codebook during training. To illustrate the usage of different codebooks, we plotted the frequency of codebook usage in the adaptive dynamic quantization model throughout the training process. The results align closely with the data in Section 4.1. As shown in Figure 3, the adaptive dynamic quantization model, implemented with Gumbel-softmax and an attention mechanism, gradually learns the various feature distributions of the dataset and selects different codebooks. At the beginning, the model tends to choose the largest codebook for fast learning, while in the later stage of learning, it tends to choose the most suitable codebook. By the final stage of training, the codebook size with the highest usage frequency matches the codebook size that achieved the lowest reconstruction loss in the fixed codebook experiment detailed in Section 4.1. For the Diabetic Retinopathy dataset, our analysis is that the dataset itself has not been uniformly preprocessed and the distribution of different features in the dataset is not obvious (As shown in Figure 5), resulting in a lack of inclination to choose a certain codebook at the beginning of training. However, in the final stage, the model will gradually converge and tend to choose the most suitable codebook.

We plotted a comparison graph of the gradient gap produced by our method versus that produced by fixed codebooks. The results, displayed in Figure 4(left), show that the adaptive dynamic quantizer method achieves optimal reconstruction performance while maintaining low gradient gap. The size of the gradient difference depends on the magnitude of the quantization error and the smoothness of the decoding function $G(\cdot)$. The minimal change in quantization loss indicates that the decoder of the adaptive dynamic quantization model exhibits better smoothness compared to the fixed codebook model. The pattern in Figure 2(right) is clear: larger codebook sizes correspond to smaller embedding dimensions and lower quantization losses. We compared the quantization loss of the dynamic quantizer with various fixed codebooks and plotted the range of the dynamic quantizer’s quantization loss. The quantization loss resulting from our dynamic quantization method is close to that of the optimal fixed codebook, demonstrating the effectiveness of our approach. As shown in Figure 4(right), the y-axis is represented in logarithmic form for clarity.

Analysis: At the beginning of training, the model is in an exploratory phase. It is trying to learn and understand the structure of the data. Larger codebook size provide a finer granularity of representation and offer more codewords to choose from, which allows the model to capture more detailed and diverse patterns in the data. Using larger codebook size can help the model avoid early commitment to suboptimal quantization, giving it the flexibility to explore different parts of the data space. As training progresses, the model starts to specialise and optimise its parameters based on the data it has seen. The need for the fine granularity provided by the larger codebook size diminishes because

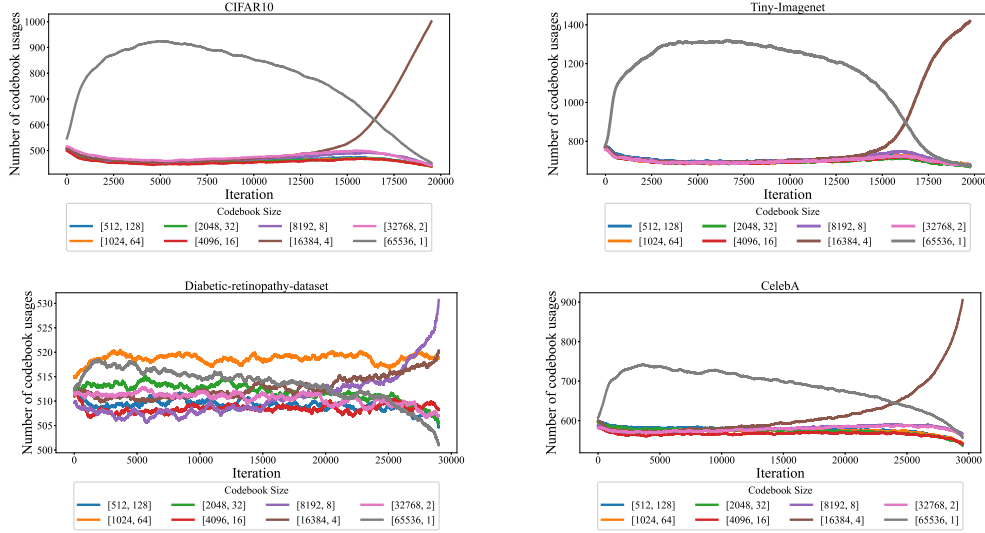


Figure 3: The frequency of adaptive selection of different-sized codebooks throughout the training process. The training can be divided into two stages: Initially, the model predominantly learns from the codebook with the most codewords; Subsequently, the model optimizes and increasingly selects the type of codebook with the minimum reconstruction loss in the fixed codebook model. The experimental results on the Diabetic Retinopathy dataset are slightly less conspicuous, but in the final stage of training, there is still a tendency to choose the most suitable codebook

Table 3: Comparison of reconstruction performance among variants of the model that adaptively select codebooks.

Models	Datasets					
	MNIST	FshionMNIST	CIFAR10	Tiny-ImageNet	Diabetic-retinopathy	CelebA
Base	0.165	0.410	0.394	2.022	0.294	0.099
$W = 32786$	0.176	0.436	0.412	2.156	0.338	0.106
$W = 16384$	0.181	0.442	0.427	2.207	0.337	0.108
$W = 8192$	0.191	0.447	0.427	2.329	0.305	0.104
$W = 4096$	0.193	0.447	0.458	2.336	0.358	0.104
Without EMA	0.317	0.595	0.490	2.559	0.361	0.173
$\alpha = 0.5$	0.171	0.424	0.428	2.204	0.355	0.102
$\alpha = 0.75$	0.175	0.442	0.440	2.482	0.325	0.104
$\alpha = 1.0$	0.188	0.492	0.466	2.387	0.380	0.118
$\alpha = 5$	0.257	0.682	0.630	3.027	0.464	0.138
$\alpha = 10$	0.271	0.823	0.700	3.278	0.485	0.182
$\beta = 0.01$	0.169	0.427	0.381	2.179	0.299	0.091
$\beta = 0.2$	0.167	0.397	0.349	1.999	0.279	0.088
$\beta = 5$	0.191	0.487	0.491	2.462	0.360	0.110
CNN	0.154	0.365	0.330	1.828	0.293	0.091
CNN+Inception	0.190	0.539	0.459	2.467	0.360	0.104

the model becomes more confident in its learned representations. They help prevent overfitting by providing a more generalised representation of the data. With fewer codewords, the model is forced to generalise better, which can lead to improved performance on unseen data. Gradually transitioning to the most suitable codebook size helps strike a balance between accurate data representation and model generalisation. For detailed mathematical proofs, please refer to the Appendix.

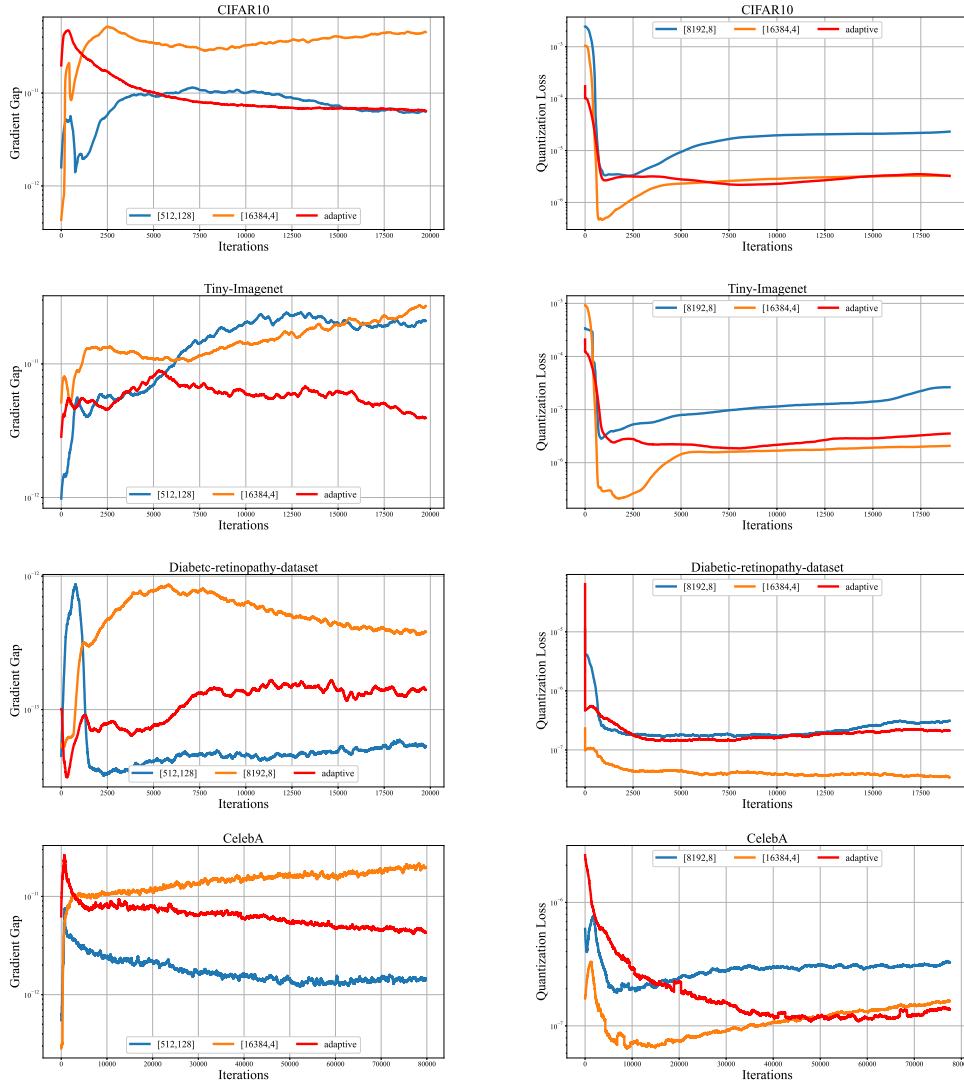


Figure 4: Comparison of quantization loss and gradient gap between adaptive dynamic quantization model and fixed codebook model. The blue color represents the model with the smallest gradient gap and the largest quantization loss in the fixed codebook model, the yellow color represents the fixed codebook model with the smallest reconstruction loss, and the red color represents the adaptive dynamic quantization model. The gradient gap and quantization loss of the adaptive quantizer are kept at low values.

4.3 Ablation study

The 'Base' model in Table 3 refers to the model discussed at the beginning of Section 4. Building on this model configuration, we conducted ablation experiments addressing various aspects such as the model's encoder-decoder structure, hyperparameters, discrete information space, and the use of EMA. Increasing the capacity of the discrete space and employing EMA to update codebooks both enhance the model's performance, with the base experiment's value of $\alpha = 0.25$ being appropriate. Across these datasets, reducing the proportion of quantization loss ($\beta = 0.2$) is shown to be beneficial. Additionally, it is noteworthy that these datasets do not require overly complex encoders and decoders. Adding ResNet and Inception layers (Szegedy et al., 2015) after the convolutional layers actually decreases model performance. The loss values in Tables 1, 2, and 3 represent the sum of reconstruction losses incurred by the model when evaluated on the respective standard validation sets of the corresponding datasets after one complete pass.

5 Conclusion

In this study, we focused on the impact of the number of codebooks and the embedding dimension on VQ-VAE's performance, with particular attention to the situation where the product of these two parameters remains constant. Our research introduced an adaptive dynamic quantizer based on Gumbel-softmax, allowing the model to adaptively choose the most ideal codebook size and embedding dimension at any given data point. It was found that the model, adopting the new method, is divided into two stages throughout the learning process. In the first stage, it tends to learn using codebooks of the largest size, while in the second stage, it gradually favors the use of the most suitable codebook. Our method demonstrated significant performance improvements in empirical validation across multiple benchmark datasets, proving the importance of adaptive dynamic discretizers for optimizing VQ-VAE models.

References

- Federico Baldassarre, Alaaeldin El-Nouby, and Hervé Jégou. Variable rate allocation for vector-quantized autoencoders. In *ICASSP 2023-2023 IEEE International Conference on Acoustics, Speech and Signal Processing (ICASSP)*, pages 1–5. IEEE, 2023.
- Gulcin Baykal, Melih Kandemir, and Gozde Unal. Edvae: Mitigating codebook collapse with evidential discrete variational autoencoders. *Available at SSRN 4671725*, 2023.
- Yoshua Bengio, Nicholas Léonard, and Aaron Courville. Estimating or propagating gradients through stochastic neurons for conditional computation. *arXiv preprint arXiv:1308.3432*, 2013.
- Prafulla Dhariwal, Heewoo Jun, Christine Payne, Jong Wook Kim, Alec Radford, and Ilya Sutskever. Jukebox: A generative model for music. *arXiv preprint arXiv:2005.00341*, 2020.
- Tanmay Gautam, Reid Pryzant, Ziyi Yang, Chenguang Zhu, and Somayeh Sojoudi. Soft convex quantization: Revisiting vector quantization with convex optimization. *arXiv preprint arXiv:2310.03004*, 2023.
- Nabarun Goswami, Yusuke Mukuta, and Tatsuya Harada. Hypervq: Mlr-based vector quantization in hyperbolic space. *arXiv preprint arXiv:2403.13015*, 2024.
- Robert Gray. Vector quantization. *IEEE Assp Magazine*, 1(2):4–29, 1984.
- Kaiming He, Xiangyu Zhang, Shaoqing Ren, and Jian Sun. Deep residual learning for image recognition. In *Proceedings of the IEEE conference on computer vision and pattern recognition*, pages 770–778, 2016.
- Minyoung Huh, Brian Cheung, Pulkit Agrawal, and Phillip Isola. Straightening out the straight-through estimator: Overcoming optimization challenges in vector quantized networks. In *International Conference on Machine Learning*, pages 14096–14113. PMLR, 2023.
- Iris Huijben, Matthijs Douze, Matthew Muckley, Ruud van Sloun, and Jakob Verbeek. Residual quantization with implicit neural codebooks. *arXiv preprint arXiv:2401.14732*, 2024.
- Lukasz Kaiser, Samy Bengio, Aurko Roy, Ashish Vaswani, Niki Parmar, Jakob Uszkoreit, and Noam Shazeer. Fast decoding in sequence models using discrete latent variables. In *International Conference on Machine Learning*, pages 2390–2399. PMLR, 2018.
- Diederik P Kingma and Max Welling. Auto-encoding variational bayes. *arXiv preprint arXiv:1312.6114*, 2013.
- Adrian Łańcucki, Jan Chorowski, Guillaume Sanchez, Ricard Marxer, Nanxin Chen, Hans JGA Dolfing, Sameer Khurana, Tanel Alumäe, and Antoine Laurent. Robust training of vector quantized bottleneck models. In *2020 International Joint Conference on Neural Networks (IJCNN)*, pages 1–7. IEEE, 2020.
- Yann LeCun, Léon Bottou, Yoshua Bengio, and Patrick Haffner. Gradient-based learning applied to document recognition. *Proceedings of the IEEE*, 86(11):2278–2324, 1998.
- Doyup Lee, Chiheon Kim, Saehoon Kim, Minsu Cho, and Wook-Shin Han. Autoregressive image generation using residual quantization. In *Proceedings of the IEEE/CVF Conference on Computer Vision and Pattern Recognition*, pages 11523–11532, 2022.
- Lei Li, Tingting Liu, Chengyu Wang, Minghui Qiu, Cen Chen, Ming Gao, and Aoying Zhou. Resizing codebook of vector quantization without retraining. *Multimedia Systems*, 29(3):1499–1512, 2023.
- Dianbo Liu, Alex M Lamb, Kenji Kawaguchi, Anirudh Goyal ALIAS PARTH GOYAL, Chen Sun, Michael C Mozer, and Yoshua Bengio. Discrete-valued neural communication. *Advances in Neural Information Processing Systems*, 34:2109–2121, 2021.
- Dianbo Liu, Alex Lamb, Xu Ji, Pascal Notsawo, Mike Mozer, Yoshua Bengio, and Kenji Kawaguchi. Adaptive discrete communication bottlenecks with dynamic vector quantization. *arXiv preprint arXiv:2202.01334*, 2022.

- Jonas Löhdefink, Jonas Sitzmann, Andreas Bär, and Tim Fingscheidt. Adaptive bitrate quantization scheme without codebook for learned image compression. In *Proceedings of the IEEE/CVF Conference on Computer Vision and Pattern Recognition*, pages 1732–1737, 2022.
- James MacQueen et al. Some methods for classification and analysis of multivariate observations. In *Proceedings of the fifth Berkeley symposium on mathematical statistics and probability*, volume 1, pages 281–297. Oakland, CA, USA, 1967.
- Fabian Mentzer, David Minnen, Eirikur Agustsson, and Michael Tschannen. Finite scalar quantization: Vq-vae made simple. *arXiv preprint arXiv:2309.15505*, 2023.
- Ali Razavi, Aaron Van den Oord, and Oriol Vinyals. Generating diverse high-fidelity images with vq-vae-2. *Advances in neural information processing systems*, 32, 2019.
- Aurko Roy, Ashish Vaswani, Arvind Neelakantan, and Niki Parmar. Theory and experiments on vector quantized autoencoders. *arXiv preprint arXiv:1805.11063*, 2018.
- Christian Szegedy, Wei Liu, Yangqing Jia, Pierre Sermanet, Scott Reed, Dragomir Anguelov, Dumitru Erhan, Vincent Vanhoucke, and Andrew Rabinovich. Going deeper with convolutions. In *Proceedings of the IEEE conference on computer vision and pattern recognition*, pages 1–9, 2015.
- Yuhta Takida, Takashi Shibuya, WeiHsiang Liao, Chieh-Hsin Lai, Junki Ohmura, Toshimitsu Uesaka, Naoki Murata, Shusuke Takahashi, Toshiyuki Kumakura, and Yuki Mitsufuji. Sq-vae: Variational bayes on discrete representation with self-annealed stochastic quantization. *arXiv preprint arXiv:2205.07547*, 2022.
- Yuhta Takida, Yukara Ikemiya, Takashi Shibuya, Kazuki Shimada, Woosung Choi, Chieh-Hsin Lai, Naoki Murata, Toshimitsu Uesaka, Kengo Uchida, Wei-Hsiang Liao, et al. Hq-vae: Hierarchical discrete representation learning with variational bayes. *arXiv preprint arXiv:2401.00365*, 2023.
- Aaron Van Den Oord, Oriol Vinyals, et al. Neural discrete representation learning. *Advances in neural information processing systems*, 30, 2017.
- Ashish Vaswani, Noam Shazeer, Niki Parmar, Jakob Uszkoreit, Llion Jones, Aidan N Gomez, Łukasz Kaiser, and Illia Polosukhin. Attention is all you need. *Advances in neural information processing systems*, 30, 2017.
- Lijun Yu, José Lezama, Nitesh B Gundavarapu, Luca Versari, Kihyuk Sohn, David Minnen, Yong Cheng, Agrim Gupta, Xiuye Gu, Alexander G Hauptmann, et al. Language model beats diffusion—tokenizer is key to visual generation. *arXiv preprint arXiv:2310.05737*, 2023.
- Neil Zeghidour, Alejandro Luebs, Ahmed Omran, Jan Skoglund, and Marco Tagliasacchi. Soundstream: An end-to-end neural audio codec. *IEEE/ACM Transactions on Audio, Speech, and Language Processing*, 30:495–507, 2021.
- Chuanxia Zheng and Andrea Vedaldi. Online clustered codebook. In *Proceedings of the IEEE/CVF International Conference on Computer Vision*, pages 22798–22807, 2023.

A Appendix

A.1 Experimental details

Diabetic Retinopathy dataset consists of a total of 2750 images belonging to five different categories of symptoms. All images have a size of 256×256 pixels. During the experiments, we selected 250 images as a validation set, following a proportional distribution among the five categories. The remaining 2500 images were used as the training set. Figure 5 shows some example images from this dataset. The CelebA dataset we used in all experiments was 8000 images extracted from official sources, extract 1000 images from each of the eight attributes, with 920 images from each category as the training set and 80 images as the validation set. Regarding training, due to the limitation of computer memory, the batch sizes for MNIST, FashionMNIST, and CIFAR10 are all set to 64. For Tiny-imagenet, CelebA and Diabetic-retinopathy-dataset, the batch sizes are set to 24, 2 and 1 respectively. The learning rate for model training in the experiment is set to $1e-4$, and the Adam optimizer is used. The temperature in the Gumbel-softmax function decreases as training progresses and kept at 1 during validation. Assuming m represents the m -th batch of training that the model is currently undergoing, then $Temperature_{training} = (iterations - m) + 1, Temperature_{validation} = 1$.



Figure 5: Sample images of Diabetic Retinopathy dataset. Left: Original image. Right: Reconstructed image.

A.2 Result analysis and proof

In Figure 1, we clearly demonstrate how to utilize the multi-head attention mechanism and the Gumbel-Softmax method to implement the dynamic selection of quantization codebooks in the model. Of course, the candidate codebook items are limited, as having too many quantization codebooks would make the model complex and consume computational resources. Figure 6 shows the experimental results on two single channel datasets. Here, we provide our analysis based on our

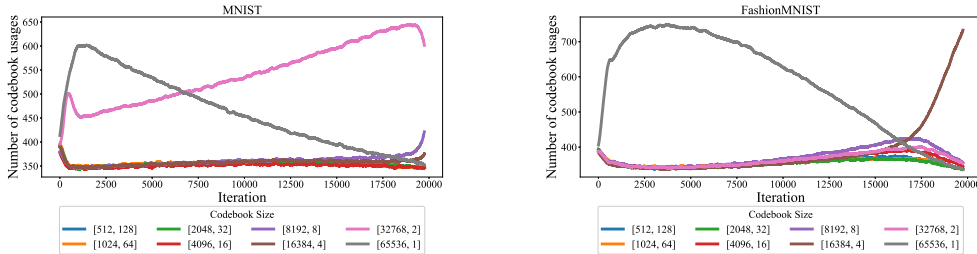


Figure 6: The frequency of selecting different codebooks during training of the adaptive dynamic quantization model on single channel datasets. Our experimental results are very consistent across five official datasets, where the adaptive codebook quantizer always manages to find the most suitable fixed codebook for its dataset at the last stage of learning.

experimental results.

Reconstruction Loss Definition: Given a dataset $\mathcal{X} = \{\mathbf{x}_i\}_{i=1}^n$ where $\mathbf{x}_i \in \mathbb{R}^M$, the reconstruction loss L using vector quantization is defined as:

$$L = \frac{1}{n} \sum_{i=1}^n \|\mathbf{x}_i - \hat{\mathbf{x}}_i\|^2 \quad (6)$$

where $\hat{\mathbf{x}}_i$ is the nearest codebook vector to \mathbf{x}_i .

Representational Capacity: The representational capacity of a codebook depends on its size N and dimensionality D . We introduce a constant K representing the inherent complexity of the data:

$$C \propto K \cdot N \cdot D \quad (7)$$

where K is proportional to the data's intrinsic dimensionality and variability.

Quantization Error with Large Codebook Size: As the codebook size N increases, the model starts to memorize the training data. This memorization can be quantified by the variance in the reconstruction error. Let V represent the variance of the data:

$$\text{Quantization Error} \propto \frac{V}{N} \quad (8)$$

Representation Error Due to Reduced Dimensionality : When N increases, D often decreases to keep the overall complexity manageable. As D decreases, the ability of the codebook vectors to represent the data reduces. The reconstruction error due to reduced dimensionality can be expressed with a constant α , reflecting the complexity of the data:

$$\text{Representation Error} \propto \frac{\alpha}{D} \quad (9)$$

Assuming $D = \frac{\beta}{N}$ (where β is a constant related to the total codebook capacity), we get:

$$\text{Representation Error} \propto \frac{\alpha N}{\beta} \quad (10)$$

Total Reconstruction Loss: The total reconstruction loss L is a combination of the errors due to quantization and reduced representation:

$$L \propto \frac{V}{N} + \frac{\alpha N}{\beta} \quad (11)$$

Incorporating Constants and Minimizing Loss: Let's incorporate the constants K , V , α , and β :

$$L = \frac{V}{N} + \frac{\alpha k N}{\beta} \quad (12)$$

To find the optimal codebook size $N_{optimal}$, we take the derivative of L with respect to N and set it to 0:

$$\frac{dL}{dN} = -\frac{V}{N^2} + \frac{\alpha K}{\beta} = 0 \quad (13)$$

Solving for N , we get:

$$\frac{V}{N^2} = \frac{\alpha K}{\beta} \quad (14)$$

$$N_{optimal} = \sqrt{\frac{V\beta}{\alpha K}} \quad (15)$$

Behavior Beyond the Optimal Point: For N beyond $N_{optimal}$:

$$N_{optimal} = \sqrt{\frac{V\beta}{\alpha K}} \quad (16)$$

When $N > N_{optimal}$, the term $\frac{\alpha K N}{\beta}$ dominates, leading to an increase in reconstruction loss L . Thus:

$$L \propto \frac{\alpha K N}{\beta} \quad (17)$$

This refined proof demonstrates that the reconstruction loss L initially decreases with increasing codebook size N due to improved data representation. However, beyond a certain point, further increasing N leads to higher loss due to:

- **Quantization Error:** Captured by the term $\frac{V}{N}$, indicating that as N increases, the model becomes too specific to the training data, increasing reconstruction loss on new data.
- **Representation Error:** Captured by the term $\frac{\alpha K N}{\beta}$, indicating that as D (which is inversely proportional to N) decreases, the codebook vectors cannot adequately capture the data complexity, leading to increased reconstruction loss.

A.3 Limitation

- **Research on Generative Models:** Our research method mainly focuses on exploring and optimizing reconstruction performance. Although significant achievements have been made in exploring this direction, we must acknowledge that due to the concentration of research objectives, we have not conducted equally in-depth research on optimizing generation performance. This is a research direction for our future work.
- **Finite Discrete Codebook Space:** We conducted our research under limited computing resources. Further exploration is needed to determine what happens when the discrete codebook space is larger and there are more codebook options available. Perhaps there will be more training stages and more optimal selection options

A.4 Additional supplementary materials for experiments

Equation 5 mentions that gradient gap measures the gradient difference between the non-quantized model and the quantized model. When the gap is 0, gradient descent with STE ensures that the loss is minimized. However, when the gap is large, this guarantee cannot be maintained. We hope to reduce such gradient gap without causing a crash in the codebook.

Figure 7 illustrates the variation of gradient gap for fixed codebook models across several datasets. Combining the experimental results provided for CIFAR10 in Section 4, we observe that the gradient gap differ between single-channel and three-channel datasets. Naturally, we lean towards acknowledging the three-channel dataset. The model has an excessively high gradient gap during the early stages of training on the single-channel dataset. Therefore, we omitted the gradient gap for the first 1000 batches of training and plotted the subsequent curves as shown in Figure 8.

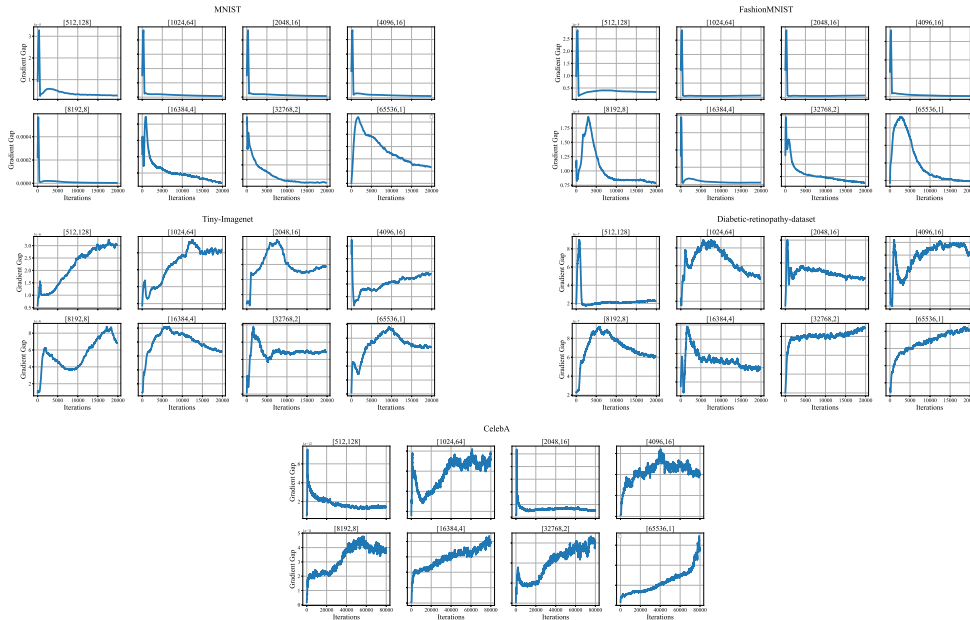


Figure 7: Gradient gap for fixed codebook models. Recording gradient gap variations during training for each dataset under each fixed codebook, with the discrete information space being constant at 65536.

It can be observed that the gradient gap on single-channel datasets exhibits a decreasing trend throughout the entire training process. However, the gradient gap curve on the three-channel dataset shows less apparent variations. We further illustrate this comparison through Figure 9(Left). On the standard three-channel dataset, the model utilizing dynamic quantization not only exhibits better reconstruction performance compared to the conventional fixed codebook model but also demonstrates low gradient gap. However, such advantages are not as pronounced on single-channel datasets. Due to the relatively small batch size, we speculate that the reason for the different patterns of gradient

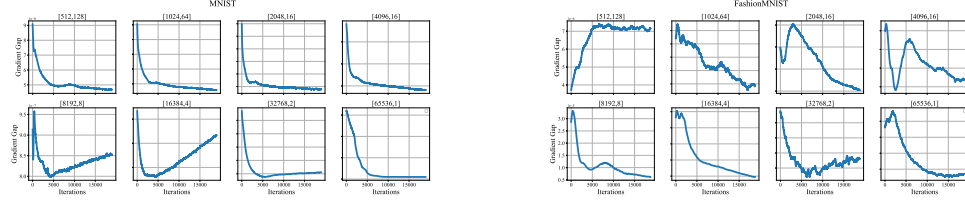


Figure 8: The gradient gap variations of the fixed codebook VQ-VAE model on single-channel datasets.

error variation is the low data complexity of single channel datasets. From Figure 9(Right), it can be seen that the quantization loss of the adaptive dynamic quantization model is similar on all six datasets, approaching the quantization loss of the optimal fixed codebook. Nonetheless, it is evident that our adaptive dynamic approach enhances the reconstruction performance of the VQ-VAE model.

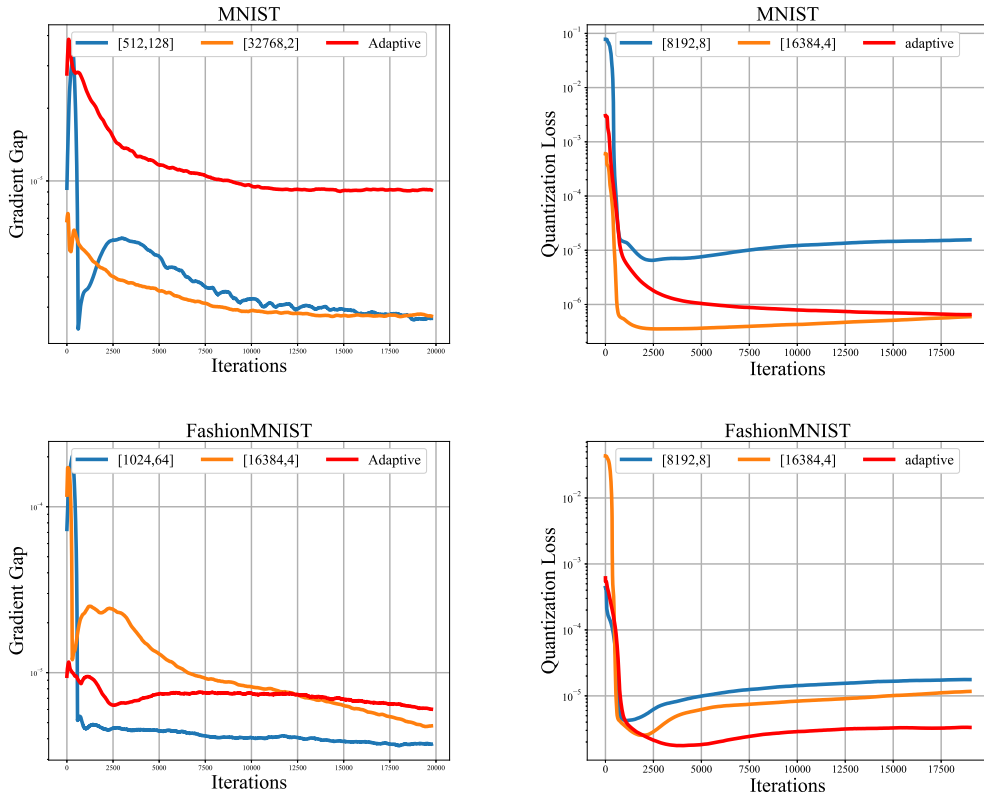


Figure 9: Comparison of gradient gap and quantization loss between the dynamic quantization model and the fixed codebook model. Left: Each plot contains three curves: the blue curve represents the lowest gradient gap in the fixed codebook model, the orange gap represents the gradient gap with the best reconstruction performance in the fixed codebook model, and the red curve represents the gradient gap in the dynamic quantization model. Right: Similar to the left figure, but the data represented is the quantization loss.

A.5 Statement

We guarantee that our research and paper strictly adhere to NeurIPS Code of Ethics.

A.6 Acknowledgement

We would like to express our deep gratitude to the authors of the original model VQ-VAE. Their model provides valuable foundation and inspiration for our research. In addition, we would like to thank other relevant researchers for providing code. URL: <https://github.com/zalandoresearch/pytorch-vq-vae?tab=MIT-1-ov-file>. License: MIT license.

This figure "best.png" is available in "png" format from:

<http://arxiv.org/ps/2407.04939v1>

This figure "cifar.png" is available in "png" format from:

<http://arxiv.org/ps/2407.04939v1>

This figure "fashion.png" is available in "png" format from:

<http://arxiv.org/ps/2407.04939v1>

This figure "mnist.png" is available in "png" format from:

<http://arxiv.org/ps/2407.04939v1>